Spike frequency adaptation mediates looming stimulus selectivity in a collision-detecting neuron

Simon Peron[1] and **Fabrizio Gabbiani**[1,2]

1 *Department of Neuroscience, Baylor College of Medicine, One Baylor Plaza, Houston, Texas 77030, USA*

2 *Department of Computational and Applied Mathematics, Rice University, 6100 Main Street MS 134, Houston, Texas 77005 USA*

Abstract

How active membrane conductance dynamics tunes neurons for specific time-varying stimuli remains poorly understood. We studied the biophysical mechanisms by which spike frequency adaptation shapes visual stimulus selectivity in an identified visual interneuron of the locust. The lobula giant movement detector (LGMD) responds preferentially to objects approaching on a collision course with the locust. Using calcium imaging, pharmacology and modeling, we show that spike frequency adaptation in the LGMD is mediated by a Ca^{2+}-dependent potassium conductance closely resembling those associated with 'small-conductance' (SK) channels. Intracellular block of this conductance minimally affected the LGMD's response to approaching stimuli, but substantially increased its response to translating ones. Thus, spike frequency adaptation contributes to the neuron's tuning by selectively decreasing its responses to nonpreferred stimuli. Our results identify a new mechanism by which spike frequency adaptation may tune visual neurons to behaviorally relevant stimuli.

Collision avoidance is crucial to an animal's survival, in the contexts of both locomotion and escape. Neural circuitry mediating collision avoidance must be tuned to approaching and not translating visual stimuli, as only the former should reliably elicit collision-avoidance behaviors. In the visual system of orthopteran insects such as locusts, two identified neurons are thought to be important in mediating such behaviors. The LGMD[1] is a higher-order visual interneuron located in the third neuropil of the optic lobe that receives input from an entire visual hemifield[2]. The LGMD outputs, with one-to-one spike correspondence, onto the descending contralateral movement detector (DCMD), a neuron having the largest axon in the locust nerve cord and projecting to motor centers involved in flight steering and jump escape behaviors[3].

The preference of the LGMD/DCMD system for objects approaching on a collision course with the insect—or their two-dimensional representations, looming stimuli[4–7]—combined with the DCMD's morphology and connectivity, strongly suggest that this system is involved in visually guided escape behavior and locomotion. Indeed, the LGMD and DCMD are exquisitely tuned to a key property of looming stimuli: their firing rate peaks reliably a fixed delay after the stimulus exceeds a threshold angular size on the eye[8,9]. Behaviorally, it has been demonstrated that the timing of the phases of the locust jump also occur after the crossing of fixed angular threshold sizes[10]. In other animals, similar looming responses have been observed both behaviorally[11] and electrophysiologically[12,13]. Despite the pervasiveness of

looming-selective neurons and behaviors across species, the biophysical mechanisms underlying this selectivity remain poorly understood. Because the LGMD/DCMD system is amenable to a variety of electrophysiological techniques *in vivo*, it represents an excellent model system for studying the underlying biophysics of neural computations mediating collision-avoidance behaviors.

Two known processes that contribute to declining firing rates in the LGMD during sustained stimulation are feed-forward inhibition[14,15] and spike-frequency adaptation[16]. Feed-forward inhibition is transiently activated in response to large and rapid luminance changes[14] and is therefore unlikely to contribute to the sustained suppression of the responses to translating objects. Though the role of spike-frequency adaptation in the response of the LGMD to visual stimuli has not yet been investigated, it may give rise to selectivity for looming versus translating stimuli: a translating stimulus activates a constant number of photoreceptors per unit time as it crosses the visual field, making it potentially susceptible to adaptation; in contrast, a looming stimulus activates a rapidly increasing number of photoreceptors as it expands, which in principle could allow it to overcome adaptation. To be effective, such adaptation would have to occur on a timescale fast enough to shut off the translating response but slow enough to allow a looming response to build up. Phenomenologically, spike-frequency adaptation in the LGMD is similar to the intermediate (medium)-duration adaptation observed in many neurons[16]. As it takes about a hundred milliseconds to activate fully, the observed adaptation could potentially satisfy the aforementioned timescale constraints. Therefore, we first investigated the biophysical mechanisms underlying spike-frequency adaptation in the LGMD. Next, we directly examined the effect of adaptation on the LGMD's response to various classes of visual stimuli *in vivo*. Finally, we were able to reproduce the visual responses using a model implementing spike-frequency adaptation. Our results suggest that adaptation is indeed involved in shaping the LGMD's selectivity for looming relative to translating stimuli, revealing a new mechanism by which spike-frequency adaptation may affect the processing of sensory stimuli.

RESULTS

LGMD responds better to looming than translating stimuli

The LGMD consists of a large dendritic field (A) thought to receive ~15,000 retinotopic, motion-sensitive excitatory inputs, and two smaller fields (B, C), each receiving ~500 feed-forward inhibitory inputs best activated by large luminance transients (Fig. 1a). The spike initiation zone is located ~260 μm from the base of field A (ref. 17). The LGMD and its postsynaptic partner the DCMD respond vigorously and reproducibly to looming stimuli (Fig. 1b). Such stimuli elicit a rapid increase in firing, with peak rates often in excess of 300 spikes s^{-1} and spike counts ~50. In contrast, translating stimuli usually elicit brief onset transients (~50 spikes s^{-1}) followed by much lower sustained firing rates (Fig. 1c), independent of velocity, size, aspect ratio and direction of motion (Fig. 1d,e). For example, the ~20 spikes observed during the translating motion depicted in Figure 1c constitute less than half of those obtained over 400 ms for a looming stimulus (Fig. 1b), despite a much longer presentation time. Thus, the mean firing rate for a looming stimulus over the last 400 ms of approach amounts to ~100 spikes s^{-1}, compared to ~10 spikes s^{-1} for a translating stimulus.

Rotating discs[2], translating gratings[14] and expanding edges[6] also elicit weaker responses than looming stimuli. Furthermore, looming stimuli elicit vigorous motor responses, well correlated with LGMD and DCMD activity[10,18], whereas translating stimuli do not[19]. These results therefore suggest that the LGMD is tuned to convey behaviorally relevant, looming-related information to downstream motor centers responsible for escape behaviors.

SK-like K⁺ conductance mediates spike-frequency adaptation

Because spike-frequency adaptation (SFA) has been observed in the LGMD[16], we hypothesized that it could suppress responses to translating stimuli. To test this hypothesis, we first sought to characterize the biophysical mechanisms underlying SFA.

During depolarizing current pulses, the LGMD's firing rate adapts and an after-hyperpolarization (AHP) is observed upon current injection termination (Fig. 2a, top). Intracellular iontophoresis of the calcium chelator BAPTA[20] caused a decrease in SFA and AHP magnitude, implying a calcium dependent process (Fig. 2a, bottom). In the LGMD, SFA is characterized as a function of current amplitude by the initial firing rate (f_0), the steady-state firing rate (f_{ss}) and the adaptation time constant (τ_{adapt}), obtained by fitting an exponential to the instantaneous firing rate's decay[16] (Fig. 2b). After BAPTA iontophoresis, f_0 remained largely unchanged (Fig. 2c), whereas f_{ss} increased (Fig. 2b,d). The time constant of adaptation, τ_{adapt}, also increased: in the case of the +8 nA current pulse illustrated in Figure 2b, it had values of 7.9 ± 2.4 ms and 13.9 ± 4.4 ms before and after BAPTA iontophoresis, respectively (mean ± s.e.m., $N = 10$ trials, $P = 1.83 \times 10^{-4}$; Wilcoxon rank-sum test). Concurrently, the AHP declined considerably (Fig. 2e). When averaged across current levels and individual locusts, BAPTA had no statistically significant effect on f_0 relative to control (Fig. 2f), but produced an increase in f_{ss} (Fig. 2g) and a reduction in AHP (Fig. 2h; Supplementary Fig. 1 online shows data for individual locusts). We corroborated the calcium dependence of SFA by perfusing the brain with saline containing the voltage-gated calcium channel blocker cadmium (Cd^{2+}, Methods). Like BAPTA, it caused an increase in f_{ss} and a reduction in AHP (Fig. 2g,h; see Supplementary Fig. 2 online for single-locust data). In contrast to BAPTA, Cd^{2+} produced a decrease in f_0 and broadened the action potentials (compare insets in Fig. 2c and Supplementary Fig. 2a), suggesting it had effects on another, BAPTA-insensitive mechanism. On average, the relative adaptation[16], $F_{adapt} = (f_0 - f_{ss})/f_0$, decreased from 0.82 ± 0.02 to 0.69 ± 0.02 in the BAPTA and Cd^{2+} experiments (mean ± s.e.m., $N = 10$ locusts; $P = 0.001$).

These experiments demonstrated that a calcium-dependent hyperpolarizing conductance contributed to SFA. Such conductances often produce a prominent AHP[21], and the effects of BAPTA and Cd^{2+} suggested that the LGMD's AHP was similarly mediated. Several more arguments support this hypothesis. First, the relative level of adaptation, F_{adapt}, after intracellular current injection in the LGMD[16] was well correlated with AHP magnitude ($\rho = -0.60$, $N = 23$ locusts). Second, the change in AHP magnitude after treatment with BAPTA or Cd^{2+} was highly correlated with the change in F_{adapt} ($\rho = 0.76$; $N = 10$ locusts). Finally, if the AHP is governed by the same mechanism as adaptation, the time constant of AHP recovery, τ_{AHP}, will be determined by the time constant governing the decline in free calcium, τ_{Ca} (ref. 22). In the LGMD, SFA in response to intracellular current injection has been shown to conform to a model allowing a direct estimation of τ_{Ca} (refs. 16,23). As observed previously[16], τ_{AHP} (126.3 ± 8.9 ms) and τ_{Ca} (132.3 ± 7.4 ms) proved to have indistinguishable values (mean ± s.e.m., $N = 23$ locusts, $P = 0.843$; Wilcoxon rank-sum test). These results allowed us to use the AHP to distinguish between two classes of calcium-dependent hyperpolarizing conductances that could mediate both SFA and the AHP in the LGMD: calcium-dependent potassium (K_{Ca})[24] and chloride (Cl_{Ca})[25] conductances. We depolarized the neuron from a slightly hyperpolarized holding potential before and after perfusion with high-potassium saline. After perfusion, the AHP was abolished, indicating that SFA was mediated by K_{Ca} ($N = 3$ locusts; Supplementary Fig. 3 online).

We next investigated the type of K_{Ca} channels involved. The kinetics of adaptation and AHP recovery were consistent with those of systems wherein intracellular calcium interacting with K_{Ca} channels of small conductance (SK) drives adaptation and AHP recovery (refs. 21,26). Though SK channels are known to be present in insects, the most common antagonist, apamin, has so far proven ineffective[27]. Consistent with this, no effect on SFA was produced by apamin

(Fig. 2f–h). Additionally, several SK antagonists and agonists failed to produce an effect (Supplementary Pharmacology and Supplementary Fig. 4 online). To rule out the involvement of the other types of K_{Ca} channel (BK and IK), we used the BK and IK blocker charybdotoxin (ChTX), known to be effective in locust neurons[28]. Like Cd^{2+}, ChTX reduced f_0 (Fig. 2f) and broadened the action potential (Supplementary Fig. 2), suggesting the presence of a BK conductance, which is known to act on the submillisecond timescale and shape the action potential and f_0 (ref. 29). This also makes it unlikely that diffusion failure explains the apamin insensitivity, as ChTX has a similar molecular weight. The slight increase in f_{ss} observed with ChTX is probably due to its effect on f_0, as reducing f_0 will result in reduced calcium influx through voltage-gated calcium channels.

The lack of an effect of ChTX on the AHP and its minimal impact on f_{ss} suggest that neither BK nor IK conductances directly contribute to SFA. Thus, although we could not definitively isolate the SFA-mediating K_{Ca} conductance pharmacologically, the kinetics of SFA and the AHP, the BAPTA and Cd^{2+} sensitivity, the dependence of the AHP on extracellular K^+ concentration, and the exclusion of BK and IK channels suggest that SFA is mainly due to an SK-like conductance with nontraditional pharmacological properties.

Adaptation suppresses *in vivo* response to translation

Because BAPTA effectively suppressed SFA after intracellular iontophoresis, we used it to test the hypothesis that SFA mediates the selectivity for looming over translating stimuli *in vivo*.

Figure 3a shows an extracellular nerve cord recording and DCMD spike rasters obtained in response to translating squares before BAPTA iontophoresis. For trials obtained after intracellular BAPTA iontophoresis in the LGMD, spikes were obtained from the intracellular LGMD recording. BAPTA abolished the 1:1 correspondence between LGMD and DCMD spikes, presumably by means of action at the LGMD axon terminal (Fig. 3a, bottom). This demonstrates that molecules like BAPTA diffuse effectively throughout the LGMD. Furthermore, it suggests that chemical transmission predominates at this mixed electrical–chemical synapse[30], as calcium is crucial for chemical transmission[31] but reduces gap junction conductance[32]. The LGMD's firing rate increased throughout the stimulus presentation after BAPTA iontophoresis, though the relative increase for the period after the onset transient was greater (Fig. 3b). This held true across individual locusts (Fig. 3c), with a larger relative change in the mean steady-state frequency, $\langle f_\blacksquare \rangle$ (Fig. 3c), than in the maximal frequency, f_{max} (Table 1), because basal firing was much lower at steady-state. The period of sustained firing >50 spikes s^{-1} increased several-fold after BAPTA iontophoresis (Table 1).

To determine whether this phenomenon was dependent on the type of translating stimulus, we tested a range of speeds, motion directions, and shapes. We used $10° \times 10°$ squares and $10° \times 80°$ rectangles moving at $40°$, $80°$, and $160° s^{-1}$ in both anterior–posterior (A–P) and posterior–anterior (P–A) directions (Table 1; individual responses in Supplementary Fig. 5 online). We observed an increased response after BAPTA iontophoresis for every tested stimulus. The relative increase in firing for the steady-state period was always larger than for the peak rate. The steady-state firing rate change after BAPTA iontophoresis was weakest for rectangles, failing to reach statistical significance ($P < 0.05$) for $160° s^{-1}$ A–P motion (Table 1). This was presumably because these larger and faster stimuli activate feed-forward inhibition onto the LGMD[15], reducing the importance of SFA in mediating stimulus selectivity. In summary, we observed a consistent increase in response after BAPTA iontophoresis, resulting in a prolonged period of sustained firing, and supporting the hypothesis that SFA prevents the LGMD from responding to translating stimuli.

Adaptation minimally affects looming response *in vivo*

To determine the contribution of SFA to the looming response, we presented, before and after BAPTA iontophoresis, stimuli simulating approaching discs with three values of the ratio of the radius (*l*) to constant approach speed (|*v*|): *l*/|*v*| = 10, 30 and 50 ms. Although BAPTA increased the firing rate, the overall time course of the response was nearly unaffected (Fig. 4a). A statistically significant increase in f_{max} was observed only for the slowest approach (*l*/|*v*| = 50 ms); the two faster speeds (*l*/|*v*| = 10 and 30 ms) produced a significant effect on $\langle f \rangle$. In all cases, however, the relative change was much smaller than for translating stimuli and the period of sustained firing was minimally affected (Table 1). Furthermore, the overlap between the responses before and after BAPTA increased with faster approaches, a result consistent with the greater effectiveness of adaptation on slower and weaker stimuli.

The LGMD's firing rate in response to looming stimuli peaks at a fixed delay, *δ*, after the stimulus exceeds a threshold angle, θ_{thresh} (ref. 33). The time of peak, the preceding increase, and the subsequent decrease in firing rate are each related to the timing of distinct phases of jump escape in behaving locusts[10]. We therefore examined the influence of BAPTA on peak timing. We observed no significant change (Fig. 4b). Moreover, θ_{thresh} and *δ* showed no significant change after BAPTA iontophoresis (Fig. 4c). We therefore conclude that the SK-like K_{Ca} conductance does not play a substantive role in shaping the time course of the response to looming stimuli.

Ca^{2+} enters the LGMD proximal to the spike initiation zone

Having established the involvement of an SK-like K_{Ca} current in SFA, and having demonstrated its role in visual processing, we wanted to localize the underlying conductance. Theoretical arguments indicate that if SFA is acting as an inhibitory conductance, it will be most effective if the underlying conductance is localized between the excitatory inputs and the spike initiation zone[34,35] (SIZ). This is because a proximal conductance has more influence than a distal one and because on-path inhibition increases the electrotonic distance between the site of excitatory input and the SIZ.

K_{Ca} conductances require calcium for activation, usually within localized microdomains[21]. Therefore, we used imaging to localize the site of Ca^{2+} influx in the LGMD during depolarizing current injections and, by extension, the presumed location of functional K_{Ca} channels. Fig. 5a (left) shows an LGMD filled with the calcium indicator Oregon Green BAPTA-I using an electrode positioned at the base of the excitatory dendritic field. We measured background-subtracted maximal changes in fluorescence (Δ*F*/*F*) during depolarizing current pulses. We observed no calcium influx in the excitatory dendrites, despite the electrode's proximity (Fig. 5a, right). For the same neuron, we also imaged the region near the SIZ (Fig. 5b, left). A large influx of calcium was observed along the main process between the SIZ and the excitatory dendritic field (Fig. 5b, right). This result was reproduced in four other neurons (for example, Fig. 5c,d, each of which shows a different neuron), revealing that only about 100–200 μm of the main process immediately adjacent to the SIZ experienced calcium influx. Moreover, calcium influx occurred both with supra- and subthreshold depolarization (Fig. 5c and 5d, respectively), suggesting that low-voltage activated calcium channels contribute to the observed influx (on the basis of the LGMD's electrotonic structure[17], the dendritic depolarization illustrated in Fig. 5d would have produced a ~5 mV depolarization at the SIZ). The lack of any Δ*F*/*F* signal in the excitatory dendrites, despite the electrode's proximity and large back-propagating spikes, suggests that voltage-gated calcium channels are largely absent from the excitatory dendrites.

SK-like conductance model reproduces physiological response

To confirm our experimental results, we next constructed a reduced compartmental model of the LGMD (see Methods) and attempted to reproduce the *in vivo* results. SFA in the LGMD conforms[16] to the predictions of a pyramidal neuron model[23] based on an SK-like K_{Ca} conductance. We modified it to take into account the morphology of the LGMD and the Ca^{2+} imaging data in Figure 5. In addition to a dendritic and axonal compartment containing conductances responsible for spike generation, we included an intermediate compartment containing the K_{Ca} conductance and a first-order mechanism governing the decline in free calcium with time constant $\tau_{Ca} = 132$ ms (Fig. 6a, inset; see Methods). The model was able to qualitatively replicate SFA and the AHP observed in the LGMD in response to current pulses, although it showed some differences from the experimental data (Fig. 6a,b). Nonetheless, the relationships between current magnitude and f_0, f_{ss}, or AHP magnitude were well reproduced overall (Fig. 6c–e), confirming that a simple model based on an SK-like K_{Ca} conductance can largely, if not perfectly, account for the experimental responses.

To test the effectiveness of the model in reproducing visual responses, we had to simulate the effect of intracellular BAPTA iontophoresis. On the basis of the formula derived previously[23] for computing τ_{Ca} and the LGMD data shown in Figure 2, we observed that τ_{Ca} declined from 98.4 ± 11.5 ms to 70.0 ± 2.9 ms after BAPTA iontophoresis (mean $\pm$ s.e.m.; $N = 7$ current levels, $P = 0.002$; Wilcoxon rank-sum test). This suggested modeling BAPTA iontophoresis as a decrease in τ_{Ca}, resulting in a faster decline of free calcium. We found that decreasing τ_{Ca}—albeit by a larger value than observed experimentally, from 132 to 20 ms— reproduced qualitatively the responses to current injection after BAPTA iontophoresis *in vivo* (Fig. 6a–e).

After confirming our ability to approximate the current injection results, we turned our attention to the contribution the simulated K_{Ca} conductance could make to visual processing. We used parameters obtained from simulations of visual stimuli in a detailed passive compartmental model of the LGMD[17] to mimic the LGMD's response to translating stimuli before and after simulated BAPTA iontophoresis (Fig. 6f). As with the *in vivo* response, the model produced an onset transient followed by reduced firing. Elimination of feed-forward inhibition reduced this transient and completely abolished it after simulated BAPTA iontophoresis (Supplementary Fig. 6 online). Also, simulated BAPTA iontophoresis resulted in an increase in response, with a larger relative increase for the steady state component, as observed experimentally. The agreement with experimental results was obtained even though the parameters of adaptation were fit independently from those of visually stimulated excitatory synapses[17]. Finally, we simulated the response of the LGMD to looming stimuli before and after BAPTA iontophoresis (Fig. 6g). As *in vivo*, the relative increase in response was much smaller for looming stimuli. Moreover, our model reproduced the observed insensitivity to BAPTA iontophoresis of the peak time, as well as of θ_{thresh} and δ (Supplementary Fig. 7 online). Thus, the model supported our central claim: that SFA in the LGMD mediated by the SK-like K_{Ca} conductance suppresses the response to translation while having little effect on looming responses.

DISCUSSION

Our results suggest that spike-frequency adaptation (SFA) in the LGMD is mostly mediated by an SK-like calcium dependent potassium (K_{Ca}) conductance. Furthermore, we showed that this conductance suppressed the response to translating stimuli but had little effect on looming responses. Thus, SFA contributes to the selectivity of the LGMD for looming over translating stimuli.

Mechanisms contributing to SFA in neurons include calcium-activated chloride[25], calcium-activated potassium[21,24], and sodium-activated potassium[36] conductances. Our BAPTA, Cd^{2+} and high-potassium saline experiments showed the presence of a K_{Ca} conductance contributing to SFA in the LGMD. The failure of the BK and IK blocker charybdotoxin[28] to influence SFA, combined with the characteristics of adaptation in the LGMD, suggests that SFA is mediated by SK channels[16,21]. The lack of an effect of apamin and other drugs targeting SK channels (Fig. 2f–h; Supplementary Fig. 4) precludes a definitive conclusion. However, the ineffectiveness of apamin in insects is well documented[27], and the lack of effect of other SK drugs occurs under some circumstances in vertebrates as well[37]. The hypothesis of an SK-like conductance mediating SFA is further supported by results from our three-compartment model. In the model, the K_{Ca} conductance is voltage independent, with activation and deactivation kinetics controlled by calcium accumulation and clearance, respectively, as is often—though not always[38]—thought to be the case for SK channels[39,40]. The model reproduced qualitatively the main properties of SFA in the LGMD and confirmed its effect on translating stimuli. The model did not reproduce exactly all our experimental results, though this was to be expected given the reduced electrotonic structure of the simulated LGMD, its simplified calcium dynamics, and the possibility that it may lack as-yet-uncharacterized conductances.

It is likely that further mechanisms contribute to SFA because it was not entirely abolished by BAPTA or Cd^{2+}. However, the high correlation between the change in AHP and F_{adapt} after BAPTA treatment suggests that the mechanism underlying the AHP is the main contributor to SFA. Imaging revealed calcium influx to occur between the excitatory dendritic field and the spike initiation zone (Fig. 5), suggesting that the localization of the K_{Ca} conductance is optimized for maximal impact of its inhibitory effect[35]. K_{Ca} can therefore suppress spiking even with relatively strong excitation, as illustrated by our *in vivo* translating stimulus experiments. Thus, even if other mechanisms contribute to SFA, the K_{Ca} conductance is likely to be a dominant factor in shaping LGMD responses to these stimuli. Similar compartmentalized voltage-dependent calcium influx has been observed in motion-sensitive blowfly neurons[41,42], and, in some of them, a calcium-dependent adaptation mechanism is also likely to be present[43].

We demonstrated that SFA mediated by the SK-like K_{Ca} conductance is important in decreasing the response to translation. It is likely that lateral inhibition and, especially with larger stimuli, feed-forward inhibition also reduce these responses[14,15]. For instance, feed-forward inhibition is likely to contribute to the observed onset transients (Figs. 1d and 3). Indeed, the onset transients were largely abolished in our model without feed-forward inhibition (Supplementary Fig. 6). The relatively large firing rate decrease caused by SFA in response to translating stimuli was also observed in simulations without feed-forward inhibition. This, combined with the fact that smaller stimuli elicit little feed-forward inhibition[15], suggests that the SK-like K_{Ca} conductance is the main driver of selectivity against translating stimuli.

The link between calcium-dependent spike-frequency adaptation and its effect on stimulus selectivity in sensory neurons has been studied in several systems. Calcium-dependent SFA has been implicated in auditory forward masking in the cricket[22]. In flies, visual motion adaptation in tangential cells is often accompanied by a prominent AHP[44], which correlates with calcium influx[43]. In weakly electric fish, SK channels contribute to the frequency tuning of pyramidal neurons in the electrosensory lateral line lobe[45]. Finally, experimental evidence and modeling suggest that calcium-dependent SFA may be partially responsible for contrast adaptation and temporal decorrelation in primary visual cortex[46,47]. In these contexts, the computational role of SFA is to act as a high-pass filter on largely stationary inputs. Our study suggests a novel role for SFA in the context of dynamically changing inputs: SFA will select

for stimuli with temporal profiles of increasing strength. In the particular case of looming stimuli, the angular size subtended by the approaching object at the retina increases supralinearly (that is, with positive acceleration). Thus, as the approach progresses, excitation increases rapidly as an ever greater number of photoreceptors are stimulated per unit time. In the LGMD, such stimuli are able to overwhelm SFA, leading to minimal changes in response whether SFA is present or not. In contrast, visual stimuli translating at constant speed activate an approximately constant number of photoreceptors per unit time, leading to rapid adaptation. Thus, only an accelerating stimulus, such as a looming stimulus, is able to overcome adaptation. More broadly, selectivity for acceleration could also prove useful in the neural processing of a range of dynamic stimuli in visual, auditory, proprioceptive and electrosensory systems.

Electrophysiological studies have revealed a great diversity of ionic conductances and distinct neuron types showing very specific conductance distributions[48]. Studies in model systems such as the LGMD, for which relatively detailed knowledge of a behavioral role exists, reveal that the functions of individual conductances are often highly specific in their contribution to the overall neural computations carried out by their respective neurons.

METHODS

Electrophysiology

Mature female locusts (*Schistocerca americana*) were dissected as described previously[17]. Thin-walled electrodes (WPI) filled with a 2 M potassium acetate, 0.5 M KCl solution were used for LGMD recordings. In BAPTA experiments, electrodes were filled with 2 M potassium acetate, 200 mM BAPTA. BAPTA was iontophoresed intracellularly into the LGMD during ~30 min of 1 s ON, 1 s OFF, −10 nA current pulses. All recordings were carried out in discontinuous current clamp mode, with a −1 nA holding current. Extracellular DCMD recordings were obtained as described previously[8].

The LGMD was identified as the neuron whose spiking matched that of the DCMD. Current pulses lasted 500 ms, with amplitudes ranging from +2 to +20 nA in 2-nA increments. In a block, each current level was repeated 5 times, with 10-s intervals between pulses. For analysis of drug effects, the last two control and drug blocks were used to compute changes in SFA parameters. The changes observed in control rundown experiments were used as reference for statistical comparison (Fig. 2f–h and Supplementary Figs. 1 and 4).

Data were analyzed using custom MATLAB programs (MathWorks). Instantaneous firing frequency curves were calculated as described previously[16]. Averages across locusts were computed using mean relative changes across all current levels that elicited spiking before and after drug treatment. The AHP time constant was fitted as described previously[16]. To examine the relationship between F_{adapt} and AHP magnitude, as well as the change thereof, correlation coefficients were computed individually for each locust across multiple current levels; the mean of these is given. We used a threshold of 50 spikes s^{-1} to quantify the change in duration of sustained firing (Table 1) because this number corresponds approximately to the firing rate observed around the earliest behavioral stage of jump escape behaviors[10]. All statistical comparisons were carried out using a nonparametric Wilcoxon rank-sum test.

Pharmacology

Unless otherwise noted, all drugs were obtained from Sigma-Aldrich. During dissections and recordings, the brain was bathed in locust saline (165 mM Cl^-, 144 mM Na^+, 5 mM K^+, 5 mM Ca^{2+}, 5 mM Mg^{2+}, 4 mM HCO_3^-, 6.3 mM HEPES buffer, 146 mM sucrose). Cadmium saline (as before, but with 1 mM Cd^{2+}, 0 mM Ca^{2+}, 10 mM Mg^{2+}) was added using a gravity perfusion system, as was high-K^+ saline (95 mM, versus 5 mM in control). To increase $[K^+]$ without

changing $[Cl^-]$, $[Na^+]$ was reduced to 54 mM, which did not abolish spiking. Apamin (Calbiochem), scyllatoxin, UCL1684, NS309 (Tocris Biosciences) and ChTX aliquots were prepared in advance and stored at −20 °C. Apamin, scyllatoxin and ChTX were added directly to the bath in concentrated form, reaching final concentrations of 600 nM, 1 μM and 2 μM, respectively, by passive diffusion (bath volume ~5 ml). All agents were dissolved in H_2O, with the following exceptions: scyllatoxin (25 mM HEPES), UCL1684 (DMSO) and NS309 (DMSO).

Imaging

Calcium imaging was performed using a BX51WI microscope (Olympus) with a 20×, 0.95 numerical aperture objective, fluorescein isothiocyanate filter set, and Rolera XR CCD camera (QImaging) operating at 10 Hz. Cells were filled following the same iontophoresis protocol as was used for BAPTA filling in electrophysiology experiments, using electrodes containing 10 μl of a 5 mM aqueous solution of Oregon green BAPTA-I (Molecular Probes) at their tip. Electrodes were backfilled with 2 M potassium acetate. The ability of BAPTA to diffuse to the synaptic terminal, as well as the effectiveness of Lucifer yellow fills in previous studies[17], suggests that there are no problems with dye diffusion. For stimulation, we used two or three 500-ms depolarizing current amplitudes (typically, +1, +5, +9 nA), with 15-s interstimulus intervals and 3–5 repetitions per amplitude. Each pixel's $\Delta F/F$ time series was obtained by first carrying out background subtraction and then averaging over a 5×5 pixel area centered at the given pixel. Trials containing motion artifacts were excluded.

Visual stimulation

The following stimuli were presented on a cathode ray tube monitor as described previously[17]: (i) Disks approaching on a collision course with the eye and characterized by $l/|v|$ ratios of 10, 30 and 50 ms (looming stimuli). (ii) Squares and rectangles translating in AP and PA directions across 80° of visual space from an azimuth of 50 to 130°, centered at an elevation of 0° (that is, at the eye equator; coordinate system as described previously[2]). Both translating stimuli were presented at speeds of 40° s^{-1}, 80° s^{-1}, and 160° s^{-1} and subtended $10° \times 10°$ and $10° \times 80°$, respectively (azimuth × elevation; measured when the stimulus was aligned with the center of the eye, perpendicular to the longitudinal body axis). (iii) A series of $5° \times 20°$ rectangles moving in an AP direction at 40° s^{-1} ('aspect ratio' stimuli). All stimuli were dark (0.57 cd m^{-2}) on a bright background (79 cd m^{-2}), with a 45 s interstimulus interval. A block constituted of a single presentation of all 15 stimuli, and 5 blocks were presented before and after BAPTA iontophoresis (except for aspect ratio stimuli, which were presented to different locusts without BAPTA iontophoresis).

Eyes were waxed into position, with eye striations serving as reference. Eye health was regularly monitored using rotating disks[17] positioned across the visual field, and locusts whose receptive fields deteriorated were rejected. We obtained mean instantaneous firing frequency curves by averaging the individual instantaneous frequency curves of the five trials presented to the locust for a given condition, then convolving with a gaussian window ($\sigma = 20$ ms). All 25 trials ($N = 5$ locusts; $N = 5$ presentations per condition per locust) were pooled in the BAPTA versus control analysis. For translating stimuli, the steady state period refers to the time from the first local minimum after f_{max} to the time of the last frequency above 3 spikes s^{-1}.

Simulations

A detailed description of the model is provided in Supplementary Methods online. Briefly, the three simulated compartments corresponded to the dendrites, the region where the K_{Ca} conductance was localized, and the axon (Fig. 6a, inset). We used the Hodgkin-Huxley formalism to simulate I_h (inward rectifier, dendritic), I_{Ca} (allowing calcium entry in the K_{Ca} compartment), and the two action potential–generating conductances, I_{KDR} (delayed-rectifier

K^+, axonal) and I_{Na} (fast sodium, axonal). A calcium-sensitive potassium current, I_{AHP}, was also included in the K_{Ca} compartment, and the decline in free calcium was simulated using a first-order process with a time constant, τ_{Ca}, of 132 ms. The effect of intracellular BAPTA iontophoresis was simulated by reducing this value to 20 ms. The properties of these conductances were fitted to the observed physiological data (Fig. 2).

Visual stimulation was simulated using synapses whose properties were based on previously obtained estimates for excitatory input strength[17] and the relative influence of feed-forward inhibition[15]. Excitatory synaptic input arrived at the dendritic compartment, whereas inhibitory input arrived at the K_{Ca} compartment. Spontaneous excitatory and inhibitory input was added, as was a visual-input timing jitter. Model output was analyzed like experimental data, with $N = 25$ runs for all visual simulations.

Supplementary Material

Refer to Web version on PubMed Central for supplementary material.

Acknowledgements

References

1. O'Shea M, Williams JLD. The anatomy and output connection of a locust visual interneurone: the lobular giant movement detector (LGMD) neurone. J Comp Physiol 1974;91:257–266.

2. Krapp HG, Gabbiani F. Spatial distribution of inputs and local receptive field properties of a wide-field, looming sensitive neuron. J Neurophysiol 2005;93:2240–2253. [PubMed: 15548622]

3. Burrows, M. The neurobiology of an insect brain. Oxford University Press; Oxford, UK: 1996.

4. Schlotterer GR. Response of the locust descending movement detector neuron to rapidly approaching and withdrawing visual stimuli. Can J Zool 1977;55:1372–1376.

5. Rind FC, Simmons PJ. Orthopteran DCMD neuron: a reevaluation of responses to moving objects. I Selective responses to approaching objects. J Neurophysiol 1992;68:1654–1666. [PubMed: 1479436]

6. Simmons PJ, Rind FC. Orthopteran DCMD neuron: a reevaluation of responses to moving objects. II Critical cues for detecting approaching objects. J Neurophysiol 1992;68:1667–1682. [PubMed: 1479437]

7. Judge S, Rind F. The locust DCMD, a movement-detecting neurone tightly tuned to collision trajectories. J Exp Biol 1997;200:2209–2216. [PubMed: 9320123]

8. Gabbiani F, Krapp HG, Laurent G. Computation of object approach by a wide-field, motion-sensitive neuron. J Neurosci 1999;19:1122–1141. [PubMed: 9920674]

9. Matheson T, Rogers SM, Krapp HG. Plasticity in the visual system is correlated with a change in lifestyle of solitarious and gregarious locusts. J Neurophysiol 2004;91:1–12. [PubMed: 13679397]

10. Fotowat H, Gabbiani F. Relationship between the phases of sensory and motor activity during a looming-evoked multistage escape behavior. J Neurosci 2007;27:10047–10059. [PubMed: 17855619]

11. Yamamoto K, Nakata M, Nakagawa H. Input and output characteristics of collision avoidance behavior in the frog *Rana catesbeiana*. Brain Behav Evol 2003;62:201–211. [PubMed: 14573994]

12. Sun H, Frost BJ. Computation of different optical variables of looming objects in pigeon nucleus rotundus neurons. Nat Neurosci 1998;1:296–303. [PubMed: 10195163]

13. Preuss T, Osei-Bonsu PE, Weiss SA, Wang C, Faber DS. Neural representation of object approach in a decision-making motor circuit. J Neurosci 2006;26:3454–3464. [PubMed: 16571752]

14. Rowell CHF, O'Shea M. The neuronal basis of a sensory analyser, the acridid movement detector system. IV The preference for small field stimuli. J Exp Biol 1977;68:157–185. [PubMed: 894184]

15. Gabbiani F, Cohen I, Laurent G. Time-dependent activation of feed-forward inhibition in a looming-sensitive neuron. J Neurophysiol 2005;94:2150–2161. [PubMed: 15928055]

16. Gabbiani F, Krapp HG. Spike-frequency adaptation and intrinsic properties of an identified, looming-sensitive neuron. J Neurophysiol 2006;96:2951–2962. [PubMed: 16571737]

17. Peron SP, Krapp HG, Gabbiani F. Influence of electrotonic structure and synaptic mapping on the receptive field properties of a collision-detecting neuron. J Neurophysiol 2007;97:159–177. [PubMed: 17021031]

18. Santer RD, Yamawaki Y, Rind FC, Simmons PJ. Preparing for escape: an examination of the role of the DCMD neuron in locust escape jumps. J Comp Physiol A Neuroethol Sens Neural Behav Physiol 2008;194:69–77. [PubMed: 18030478]

19. Rowell CH. The orthopteran descending movement detector (DMD) neurones: a characterisation and review. Z vergl Physiol 1971;73:167–194.

20. Tsien RY. New calcium indicators and buffers with high selectivity against magnesium and protons: design, synthesis, and properties of prototype structures. Biochemistry 1980;19:2396–2404. [PubMed: 6770893]

21. Stocker M. Ca^{2+}-activated K^+ channels: molecular determinants and function of the SK family. Nat Rev Neurosci 2004;5:758–770. [PubMed: 15378036]

22. Sobel EC, Tank DW. *In Vivo* Ca^{2+} Dynamics in a Cricket Auditory Neuron: An Example of Chemical Computation. Science 1994;263:823–826. [PubMed: 17770837]

23. Wang XJ. Calcium coding and adaptive temporal computation in cortical pyramidal neurons. J Neurophysiol 1998;79:1549–1566. [PubMed: 9497431]

24. Faber ES, Sah P. Calcium-activated potassium channels: multiple contributions to neuronal function. Neuroscientist 2003;9:181–194. [PubMed: 15065814]

25. Scott RH, Sutton KG, Griffin A, Stapleton SR, Currie KP. Aspects of calcium-activated chloride currents: a neuronal perspective. Pharmacol Ther 1995;66:535–565. [PubMed: 7494858]

26. Bond CT, Maylie J, Adelman JP. SK channels in excitability, pacemaking and synaptic integration. Curr Opin Neurobiol 2005;15:305–311. [PubMed: 15922588]

27. Wicher D, Walther C, Wicher C. Non-synaptic ion channels in insects–basic properties of currents and their modulation in neurons and skeletal muscles. Prog Neurobiol 2001;64:431–525. [PubMed: 11301158]

28. Heidel E, Pflüger HJ. Ion currents and spiking properties of identified subtypes of locust octopaminergic dorsal unpaired median neurons. Eur J Neurosci 2006;23:1189–1206. [PubMed: 16553782]

29. Gu N, Vervaeke K, Storm JF. BK potassium channels facilitate high-frequency firing and cause early spike frequency adaptation in rat CA1 hippocampal pyramidal cells. J Physiol (Lond) 2007;580:859–882. [PubMed: 17303637]

30. Killmann F, Schürmann FW. Both electrical and chemical transmission between the lobula giant movement detector and the descending contralateral movement detector neurons of locusts are supported by electron microscopy. J Neurocytol 1985;14:637–652. [PubMed: 2415687]

31. Neher E, Sakaba T. Multiple roles of calcium ions in the regulation of neurotransmitter release. Neuron 2008;59:861–872. [PubMed: 18817727]

32. Peracchia C. Chemical gating of gap junction channels; roles of calcium, pH and calmodulin. Biochim Biophys Acta 2004;1662:61–80. [PubMed: 15033579]

33. Gabbiani F, Krapp HG, Koch C, Laurent G. Multiplicative computation in a visual neuron sensitive to looming. Nature 2002;420:320–324. [PubMed: 12447440]

34. Rall, W. Theoretical significance of dendritic trees for neuronal input-output relations. In: Reiss, RF., editor. Neural Theory and Modeling. Stanford University Press; Palo Alto, CA: 1964.

35. Koch C, Poggio T, Torre V. Retinal ganglion cells: a functional interpretation of dendritic morphology. Phil Trans R Soc Lond B 1982;298:227–263. [PubMed: 6127730]

36. Bhattacharjee A, Kaczmarek LK. For K^+ channels, Na^+ is the new Ca^{2+} Trends Neurosci 2005;28:422–428. [PubMed: 15979166]

37. Wittekindt OH, et al. An Apamin and Scyllatoxin-Insensitive Isoform of the Human SK3 Channel. Mol Pharmacol 2004;65:788–801. [PubMed: 14978258]

38. Teagarden M, Atherton JF, Bevan MD, Wilson CJ. Accumulation of cytoplasmic calcium, but not apamin-sensitive afterhyperpolarization current, during high frequency firing in rat subthalamic nucleus cells. J Physiol (Lond) 2008;586:817–833. [PubMed: 18063664]

39. Sah P. Ca^{2+}-activated K^+ currents in neurones: types, physiological roles and modulation. Trends Neurosci 1996;19:150–154. [PubMed: 8658599]

40. Hirschberg B, Maylie J, Adelman JP, Marrion NV. Gating of recombinant small-conductance Ca-activated K^+ channels by calcium. J Gen Physiol 1998;111:565–581. [PubMed: 9524139]

41. Haag J, Borst A. Spatial distribution and characteristics of voltage-gated calcium signals within visual interneurons. J Neurophysiol 2000;83:1039–1051. [PubMed: 10669515]

42. Single S, Borst A. Different mechanisms of calcium entry within different dendritic compartments. J Neurophysiol 2002;87:1616–1624. [PubMed: 11877530]

43. Kurtz R, Dürr V, Egelhaaf M. Dendritic calcium accumulation associated with direction-selective adaptation in visual motion-sensitive neurons *in vivo*. J Neurophysiol 2000;84:1914–1923. [PubMed: 11024084]

44. Harris RA, O'Carroll DC, Laughlin SB. Contrast gain reduction in fly motion adaptation. Neuron 2000;28:595–606. [PubMed: 11144367]

45. Ellis LD, et al. SK channels provide a novel mechanism for the control of frequency tuning in electrosensory neurons. J Neurosci 2007;27:9491–9502. [PubMed: 17728462]

46. Sanchez-Vives MV, Nowak LG, McCormick DA. Cellular mechanisms of long-lasting adaptation in visual cortical neurons *in vitro*. J Neurosci 2000;20:4286–4299. [PubMed: 10818164]

47. Wang XJ, Liu Y, Sanchez-Vives MV, McCormick DA. Adaptation and temporal decorrelation by single neurons in the primary visual cortex. J Neurophysiol 2003;89:3279–3293. [PubMed: 12649312]

48. Migliore M, Shepherd GM. Emerging rules for the distributions of active dendritic conductances. Nat Rev Neurosci 2002;3:362–370. [PubMed: 11988775]
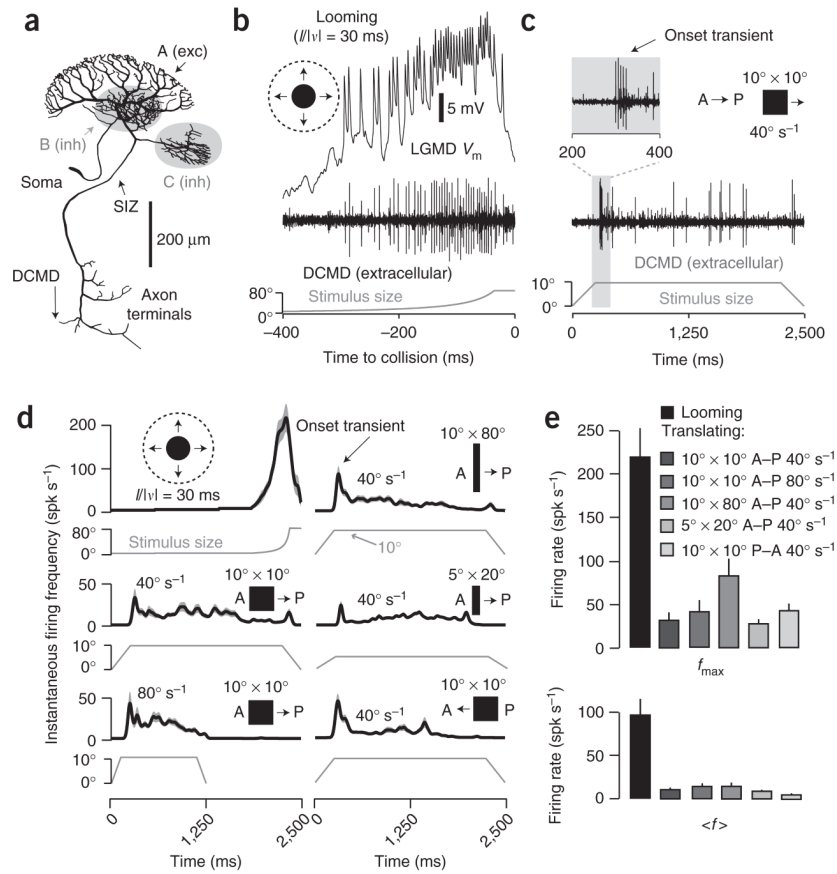
Figure 1.

LGMD morphology and response to looming versus translating stimuli. (**a**) LGMD reconstruction[17] showing excitatory (A; exc) and inhibitory (B, C; inh) dendrites. (**b**) Response to looming ($l/|v| = 30$ ms). Top, LGMD membrane potential (V_m). Middle, corresponding nerve cord recording showing DCMD spikes. Bottom, the approaching disk's retinal angle as a function of time to collision ($t = 0$). (**c**) Response to a $10° \times 10°$ square, translating at $40°$ s^{-1} in the A–P direction. The onset transient is magnified in the inset. Stimulus size is the retinal angle subtended in the azimuth direction. The initial size increase is due to the object's moving onto the screen. (**d**) Responses to assorted stimuli. Dark lines, gaussian-convolved instantaneous firing frequency (spikes s^{-1}); gray envelopes, s.e.m. ($N = 25$ trials, 5 per locust). Left column: a looming disk ($l/|v| = 30$ ms; top) and $10° \times 10°$ squares translating at $40°$ s^{-1} (middle) or $80°$ s^{-1} (bottom) in the A–P direction. Right column: $10° \times 80°$ (top) and $5° \times 20°$ (middle) rectangles translating at $40°$ s^{-1} in the A–P direction and a $10° \times 10°$ square translating at $40°$ s^{-1} in the P–A direction (bottom). (**e**) Peak (f_{max}) and mean ($\langle f \rangle$) firing rate in response to visual stimuli. $\langle f \rangle$ for looming was for the last 500 ms of approach; $\langle f \rangle$ for translation was for the steady state period (Methods). Error bars, s.e.m. ($N = 25$ trials, as in **d**); spk, spikes.
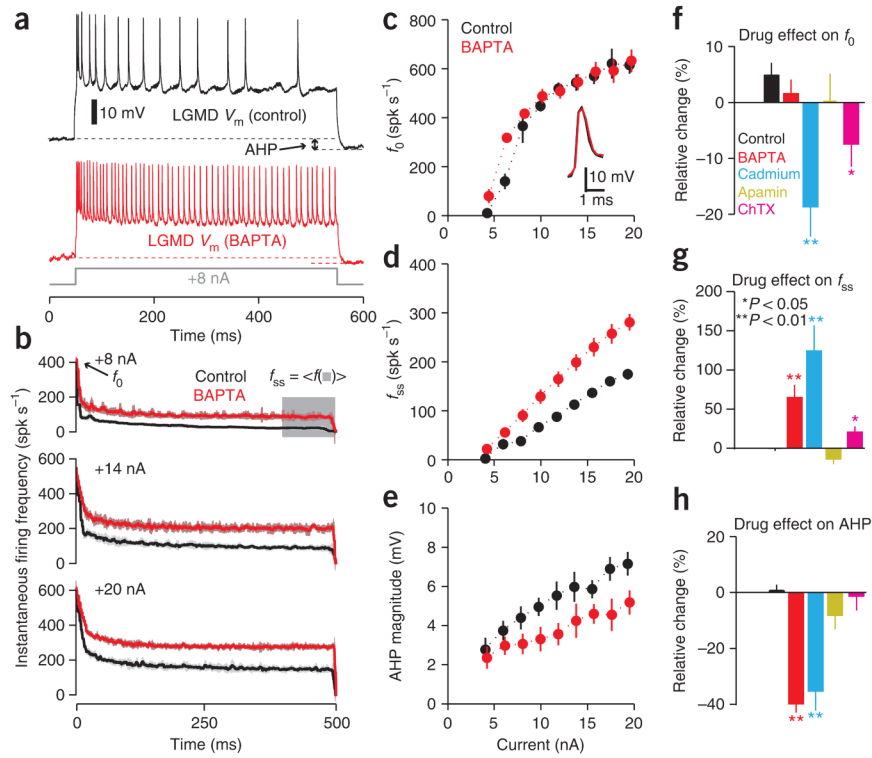
Figure 2.
Spike frequency adaptation in the LGMD results from an SK-like K_{Ca} conductance. (**a**) LGMD membrane potential (V_m) during current injection (+8 nA, 500 ms), before (black) and after (red) BAPTA iontophoresis. Arrow, example after-hyperpolarization. (**b**) Instantaneous firing rate during depolarization before (black) and after (red) BAPTA iontophoresis ($N = 10$ trials, 1 locust; s.d. envelopes). Time interval used for steady-state frequency (f_{ss}) is highlighted in gray. (**c–e**) Initial firing frequency (f_0; **c**), steady-state frequency (f_{ss}; **d**), and AHP magnitude (**e**) as a function of current before (black) and after (red) BAPTA (10 repetitions per current level; error bars, s.d.); inset, effect of BAPTA on action potential shape. (**f–h**) Summary of drug effects, obtained by measuring the mean relative change pooled across current levels triggering spiking and averaging across $N = 5$ locusts for control (rundown; see Methods), BAPTA, cadmium (Cd^{2+}) and charybdotoxin (ChTX); $N = 3$ for apamin (error bars, s.e.m.). (**f**) Cd^{2+} and ChTX reduced f_0 relative to control ($P = 0.008$ and $P = 0.032$, respectively; Wilcoxon rank-sum test). BAPTA and apamin yielded no change ($P = 0.421$ and $P = 0.393$, respectively). (**g**) BAPTA and Cd^{2+} gave rise to f_{ss} increases ($P = 0.008$ for both), as did ChTX ($P = 0.032$). Apamin had no effect ($P = 0.071$). (**h**) BAPTA and Cd^{2+} gave rise to decreases in AHP ($P = 0.008$ for both); apamin and ChTX had no effect ($P = 0.143$ and $P = 0.841$, respectively). Spk, spikes.
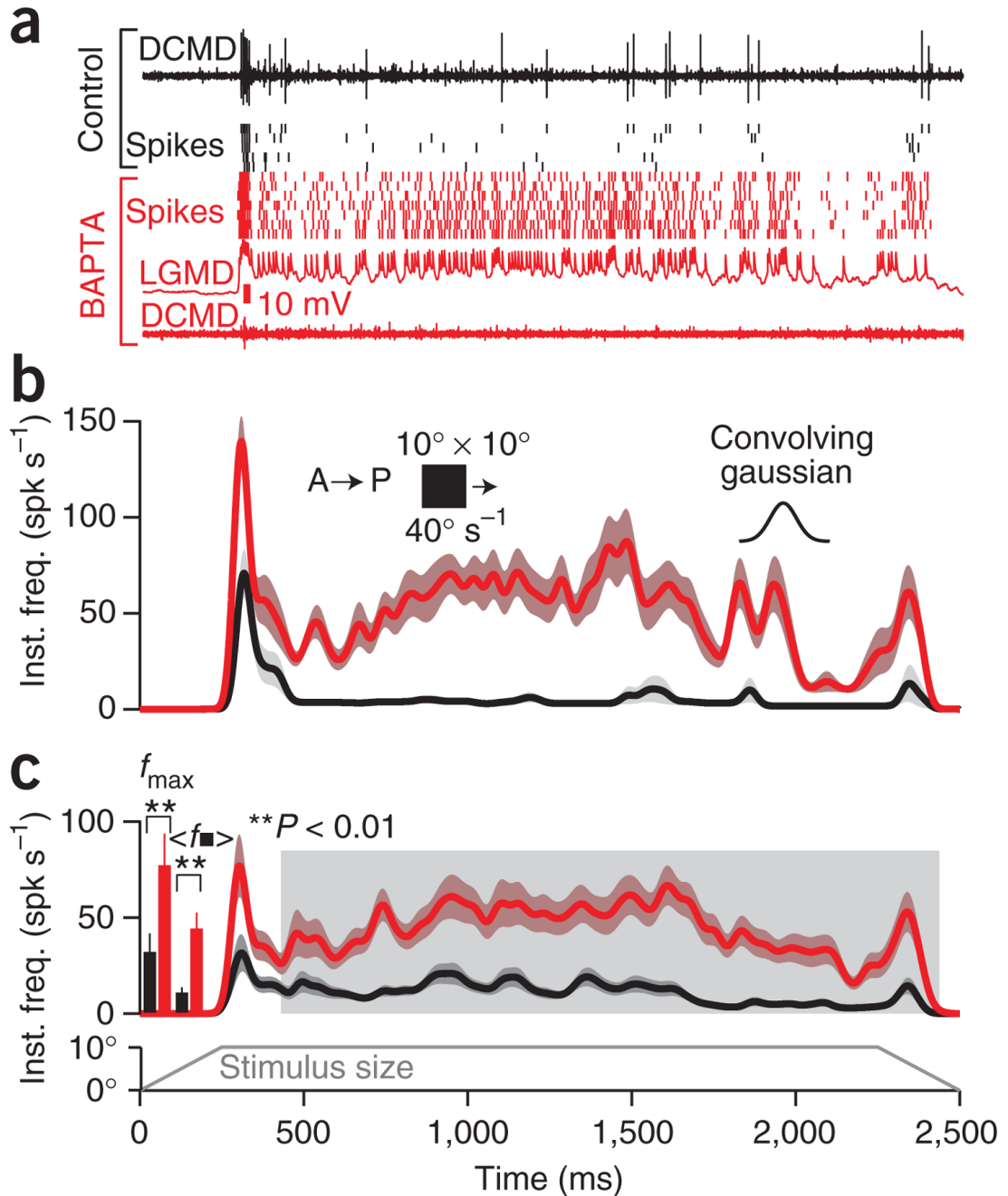
Figure 3.
Intracellular block of spike frequency adaptation (SFA) *in vivo* enhances the responses to translating motion. Stimulus consisted of a $10° \times 10°$ square translated in the A–P direction at $40°\ s^{-1}$. The size of the stimulus in the azimuth direction as a function of time is indicated at the bottom of **c**. (**a**) Top trace, extracellular nerve cord recording with DCMD spikes for a single trial. The black rasters indicate DCMD spike times for different presentations of the same stimulus. The red rasters show LGMD spike times after BAPTA iontophoresis ($N = 7$). The red nerve cord recording (bottom) was acquired simultaneously with an LGMD membrane potential trace (second from bottom); there was complete breakdown of LGMD:DCMD spike correspondence. (**b**) Gaussian-convolved (inset; $\sigma = 20$ ms) average instantaneous firing rate

(inst. freq.) for the locust in **a** before (black) and after (red) BAPTA iontophoresis. Envelopes indicate s.e.m. (**c**) Instantaneous firing rate across five locusts before and after BAPTA iontophoresis (conventions as in **b**; five trials per condition per locust, $N = 25$ total). Shaded region was used to compute steady state firing frequency, $\langle f_\blacksquare \rangle$ (Methods). Left bar plots: increase in $f_{\max}$ and $\langle f_\blacksquare \rangle$ after BAPTA iontophoresis (mean; error bars, s.e.m.; $P = 7.39 \times 10^{-4}$ and $P = 5.85 \times 10^{-9}$, respectively; Wilcoxon rank-sum test; see Table 1).
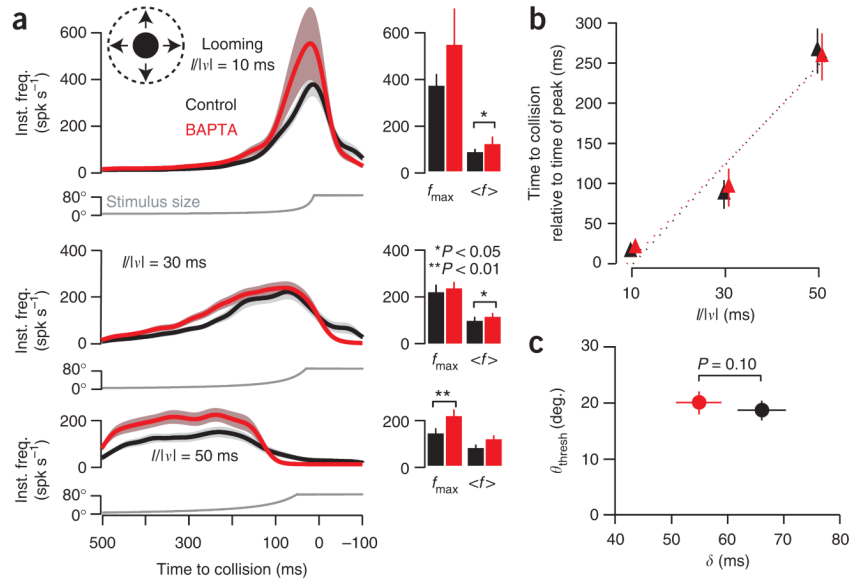
Figure 4.
Block of spike frequency adaptation has little effect on the time-course of looming response. (**a**) Responses to looming disks approaching with $l/|v| = 10$, 30 and 50 ms. Gaussian-convolved average instantaneous firing rate (inst. freq.) before (black) and after BAPTA iontophoresis (red). Envelopes indicate s.e.m. (5 locusts, 5 trials per locust per condition; $N = 25$). The bar plots depict the corresponding mean ($\langle f \rangle$) and peak (f_{max}) firing frequencies (lines indicate s.e.m.; see Table 1). The BAPTA-induced change in f_{max} was significant only for $l/|v| = 50$ ms ($P = 0.035$), whereas the change in $\langle f \rangle$ was significant for $l/|v| = 10$ and 30 ms ($P = 0.021$ and 0.033, respectively). (**b**) Firing rate peak relative to collision time for the same three $l/|v|$ values, before (black) and after (red) BAPTA. Solid lines indicate s.e.m. Dotted lines represent linear fits. Peak times after BAPTA shifted from 14.4 ± 3.1 ms (mean ± s.e.m.) to 19.3 ± 2.4 ms, 86.2 ± 17.9 ms to 94.8 ± 23.7 ms, and 265.1 ± 28.1 ms to 257.7 ± 29.3 ms for $l/|v| = 10$, 30 and 50 ms, respectively ($P = 0.15$, 1 and 1, respectively; $N = 25$). (**c**) Threshold angle (θ_{thresh}) as a function of delay to firing rate peak (δ). After BAPTA iontophoresis, θ_{thresh} shifted from $18.8° \pm 1.7°$ to $19.9° \pm 2.1°$ ($P = 1$, $N = 25$) and δ shifted from 66.1 ± 4.3 ms to 54.9 ± 4.1 ms ($P = 0.1$, $N = 25$). Same conventions as in **b**.
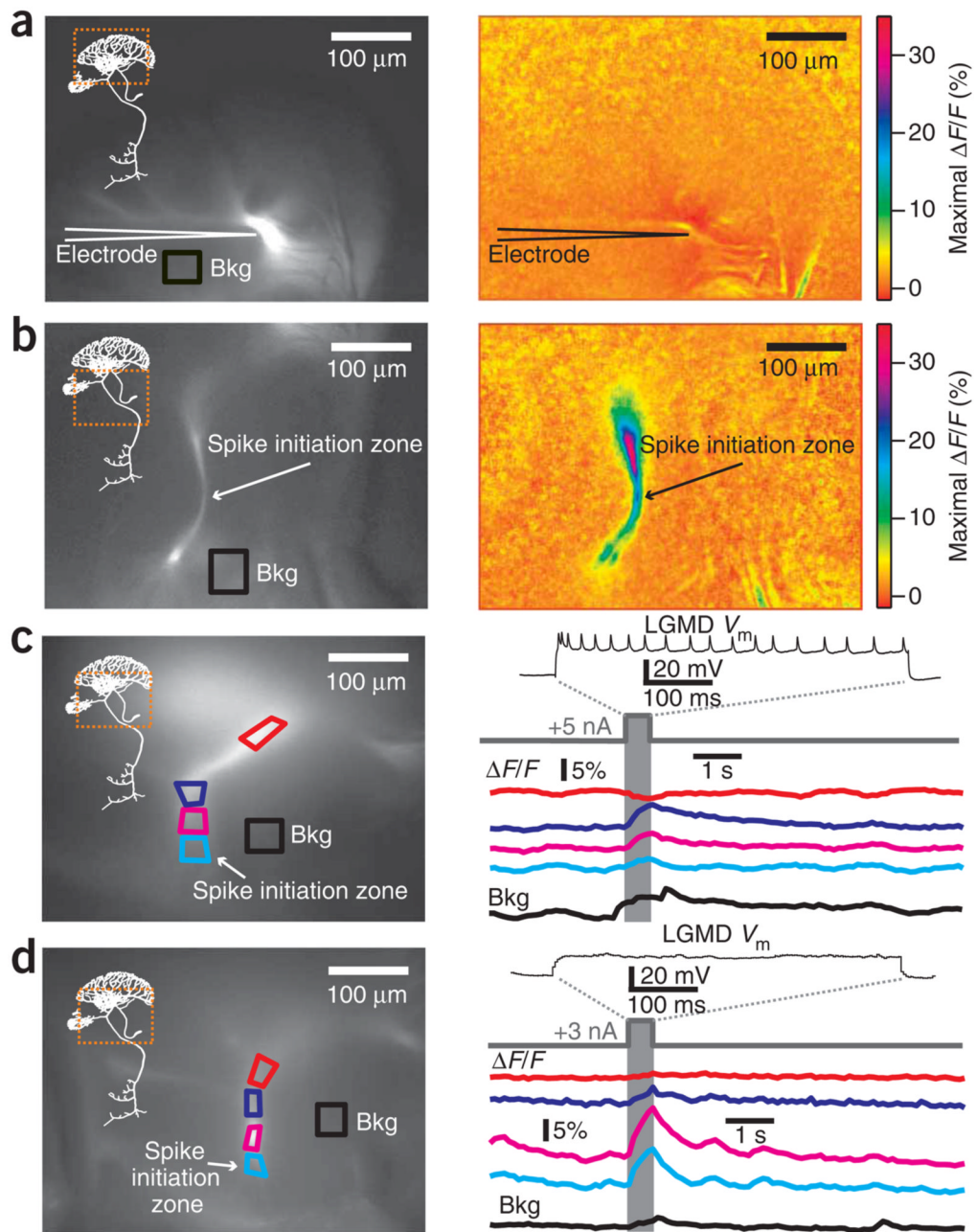
Figure 5.
Calcium entry is confined to a region of the LGMD close to the spike initiation zone during depolarizing current injection. (**a**) Basal fluorescence image of the excitatory dendritic field (left) and maximal $\Delta F/F$ (right) in response to depolarizing current (500 ms, +9 nA). Bkg, region used for background subtraction. Dashed square (left panel) shows the LGMD region imaged in right panel. (**b**) Raw fluorescence image of the SIZ (left) and maximal $\Delta F/F$ (right) for the same neuron, penetration site and current shown in **a**. (**c**) Basal resting fluorescence image of a second LGMD neuron (left), with four regions of interest (ROIs) demarcated in different colors. Top trace (right), membrane potential (V_m) during a dendritic depolarizing current pulse (500 ms, +5 nA). Colored traces, time course of $\Delta F/F$ in the ROIs. Bottom trace, $\Delta F/F$ used for background subtraction. (**d**) Basal resting fluorescence image (left) and V_m

response (right, top) in a third LGMD neuron during subthreshold dendritic current pulse (500 ms, +3 nA). The subsequent traces show $\Delta F/F$ in the ROIs indicated on the left. Calcium influx does not depend on action potential firing. Electrode is outside field of view in **b**–**d**.
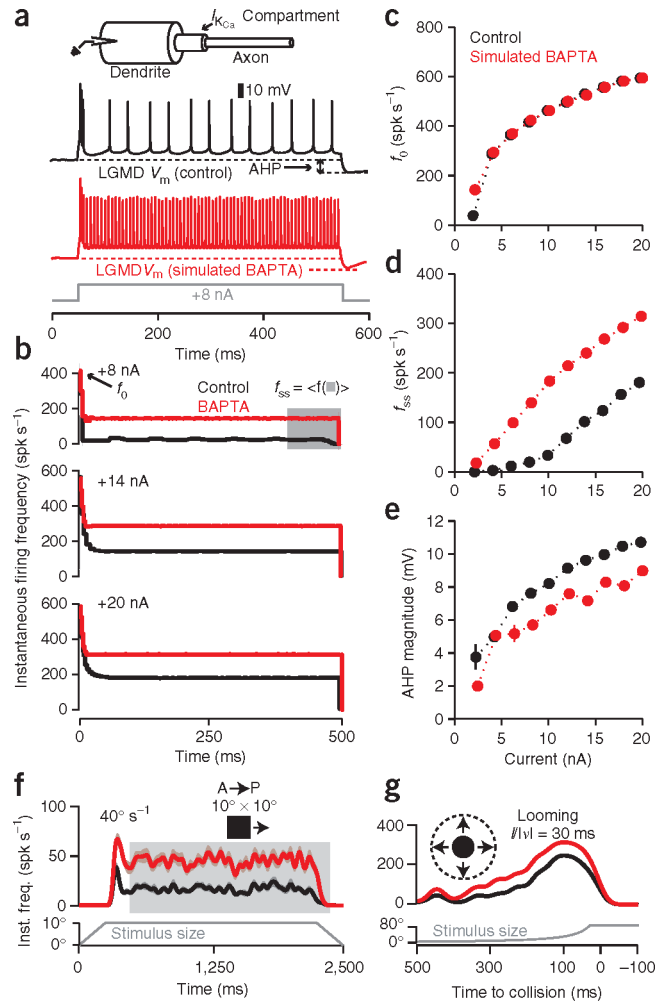
Figure 6.
LGMD compartmental model reproduces *in vivo* current injection and visual stimulation results, both before and after block of spike frequency adaptation by simulated BAPTA iontophoresis. (**a**) The model consisted of dendritic and axonal compartments connected by a K_{Ca} compartment (inset, top; see Methods). The electrode was positioned in the dendritic compartment. Membrane potential (V_m) traces show model response to a depolarizing current (500 ms, +8 nA) without (black) and with (red) simulated BAPTA iontophoresis. (**b**) The model gave rise to adaptation with a time course similar to that observed *in vivo* (Fig. 2b). (**c**–**e**) Sensitivity of SFA parameters to simulated BAPTA: f_0 did not change (**c**), whereas f_{ss} increased (**d**) and AHP declined (**e**). Error bars, s.d. ($N = 10$ repetitions per current level; see Methods). (**f**) Gaussian-convolved average response of the model to simulated translation of a $10° \times 10°$ square in the A–P direction at $40°$ s^{-1} before (black) and after (red) simulated BAPTA iontophoresis. Inst. freq., instantaneous firing rate. The f_{max} increased 103%, from 51 ± 5 to 104 ± 5 Hz, and $\langle f_{\blacksquare} \rangle$ increased 152%, from 18 ± 0.3 to 45 ± 1 Hz, after simulated BAPTA iontophoresis (mean $\pm$ s.e.m.; $N = 25$ trials, variability described in Methods). (**g**) Gaussian-convolved average response of the model to simulated looming stimulus ($l/|v| = 30$ ms) before (black) and after (red) simulated BAPTA iontophoresis: f_{max} increased 26%, from 248 ± 2 to 314 ± 1 Hz, and $\langle f \rangle$ increased 51%, from 102 ± 1 to 153 ± 1 Hz (mean $\pm$ s.e.m.; $N = 25$ trials).

Table 1

BAPTA produces a stronger increase in firing rate and longer sustained responses for translating stimuli than for looming stimuli

Stimulus class	f_{max} (spikes s^{-1})				$\langle f_\blacksquare \rangle$, $\langle f \rangle$ (spikes s^{-1})				Longest contiguous time $f > 50$ spikes s^{-1} (ms)		
	Control	BAPTA	Δ (%)	P-value	Control	BAPTA	Δ (%)	P-value	Control	BAPTA	P-value
Translating rectangles											
10°×10°, 40° s^{-1}, A–P	32 ± 5	77 ± 10	144	7 ± 10^{-4}	11 ± 1	44 ± 3	308	6×10^{-9}	30 ± 6	397 ± 66	2×10^{-9}
10°×10°, 80° s^{-1}, A–P	41 ± 7	81 ± 10	100	0.001	15 ± 2	52 ± 6	237	6×10^{-7}	40 ± 7	353 ± 63	4×10^{-8}
10°×10°, 160° s^{-1}, A–P	59 ± 6	93 ± 6	58	9×10^{-4}	18 ± 2	58 ± 7	231	1×10^{-6}	52 ± 8	260 ± 38	9×10^{-7}
10°×10°, 40° s^{-1}, P–A	42 ± 5	92 ± 6	118	2×10^{-6}	8 ± 1	31 ± 4	276	2×10^{-6}	26 ± 6	213 ± 37	1×10^{-7}
10°×10°, 80° s^{-1}, P–A	51 ± 4	100 ± 7	95	4×10^{-5}	9 ± 2	42 ± 6	353	2×10^{-6}	35 ± 6	217 ± 38	4×10^{-7}
10°×10°, 160° s^{-1}, P–A	58 ± 5	102 ± 10	77	4×10^{-4}	12 ± 2	46 ± 7	278	8×10^{-5}	40 ± 6	128 ± 20	7×10^{-5}
10°×80°, 40° s^{-1}, A–P	82 ± 9	137 ± 9	66	1×10^{-4}	16 ± 2	52 ± 7	232	6×10^{-5}	110 ± 16	651 ± 106	2×10^{-6}
10°×80°, 80° s^{-1}, A–P	81 ± 10	122 ± 9	50	0.005	11 ± 2	33 ± 6	191	0.035	83 ± 14	282 ± 57	0.034
10°×80°, 160° s^{-1}, A–P	95 ± 10	130 ± 11	37	0.044	11 ± 2	18 ± 4	58	0.461	74 ± 7	140 ± 21	0.200
Average			83				242				
Looming disks											
$l/|v| = 10$ ms	366 ± 50	541 ± 152	48	0.430	81 ± 7	116 ± 26	42	0.021	229 ± 14	245 ± 16	0.573
$l/|v| = 30$ ms	220 ± 32	236 ± 24	7	0.569	97 ± 9	114 ± 11	18	0.033	340 ± 26	375 ± 26	0.303
$l/|v| = 50$ ms	138 ± 16	211 ± 25	53	0.005	75 ± 8	112 ± 13	49	0.960	309 ± 33	306 ± 28	0.960
Average			36				36				

With the exception of the fastest-moving 10° × 80° rectangle, BAPTA produced significant increases for both maximal response frequency, f_{max}, and the mean response during the steady state period, $\langle f_\blacksquare \rangle$, for all translating stimuli. The relative increase in looming response was much smaller and significant only for the weakest stimulus ($l/|v| = 50$ ms). The longest contiguous period of sustained firing above 50 spikes s^{-1} was greatly increased for translating but not looming stimuli. All values are mean ± s.e.m. ($N = 25$ trials, pooled from 5 locusts with 5 trials each; Wilcoxon rank-sum test comparing the control (before BAPTA) with the response after BAPTA treatment. The two average rows give mean relative changes across all translating and looming conditions, respectively. Δ, percentage change of the mean after BAPTA). Δ, percentage change of the mean after BAPTA. The raw data for looming and translating stimuli are shown in Figure 4 and Supplementary Figure 5, respectively.